A PRACTICAL MODEL FOR CONTRAST UNDER NIGHTTIME, ARTIFICIAL ILLUMINATION

Donald W. Hoock Jr.
U.S. Army Research Laboratory
Information Science and Technology Directorate
Battlefield Environment Division
White Sands Missile Range, NM 88002-5501

John C. Giever
Sean G. O'Brien
Physical Science Laboratory
New Mexico State University
Las Cruces, NM 88003

ABSTRACT

Under the support of TRAC-WSMR and as a long-term research project, coordinated with the U.S. Army TRADOC-lead Target-Acquisition Simulation (ACQSIM) program, we have developed a practical model for computing the effects on target contrast of artificial illumination sources (flares) in the presence of aerosols and obscurants. In this paper we describe this parametric model and its use of multi-stream radiative transfer equations and scaling laws to provide estimation of the radiance from obscurant clouds illuminated by point-source flares. The model is based on the detailed numerical calculations of direct and terrain-reflected radiance for the unobscured environment, combined with results from the 26-stream Battlefield Emission and Multiple Scattering (BEAMS) radiative transfer model for obscurant multiple scattering. We show how the resulting modeled radiances can be used to compute target/background contrasts and effective "sky-to-ground" ratio inputs required by contrast propagation models. We also show visualization examples that illustrate the interesting scenarios that can result from the relative positions of flare. aerosol cloud, illuminated target, illuminated terrain and distant dark backgrounds.

INTRODUCTION

Sensor performance calculations are based on knowing the signal available at the sensor aperture. Target acquisition models and combat simulations thus must treat various environmental effects. These include atmospheric propagation loss, available natural and man-made illumination, atmospheric effects on the spatial or angular resolution of target details, and the effects of scattered radiance on reducing target to background contrast.

The contrast equation used in models and simulations is based on the ratio of the difference in radiance L ($W/m^2/sr$) between an object and its background, relative to that of the background:

$$c(o) = \frac{L_o(0) - L_b(0)}{Lb\ (0)} \qquad (1)$$

where C(0) is the (dimensionless) contrast at distance zero from the object, and $L_o(0)$ is the radiance ($W/m^2/sr$) from the object at range zero. $L_b(0)$ is the radiance from the background as it appears from the position of the object, regardless of how far the background actually is beyond the object.

Over a path of distance s (m) from the object to the sensor, each radiance L(0) experiences a transmission loss (signal loss) and an accumulation of in-scattered and emitted "path radiance" L_p (usually as an unwanted noise from the sensor's point of view):

$$\begin{aligned} L(s) &= T(s)\cdot L(0) + L_p(s) \\ &= T(s)\cdot L(0) + \left[1 - T(s)\right]\cdot L_s \end{aligned} \qquad (2)$$

where transmission T(s) is usually computed internally in the simulation from:

$$T(s) = \exp\left(-k_{ext} \cdot s\right) = \exp\left(-\alpha \int c(s)\, ds\right) \quad (3)$$

where k_{ext} is an input or modeled "volume extinction coefficient" (m^{-1}), α is an input extinction per unit concentration or "mass extinction coefficient" (m^2/g), and c(s) is the modeled aerosol concentration (g/m^3) over the path. As can be seen, the relationship between path radiance $L_p(s)$ over the path and transmission is:

$$L_p(s) = \left[1 - T(s)\right] \cdot L_s \quad (4)$$

"where L_s is called the average "limiting path radiance" over the path.

Substituting Eqs. 2 and 4 into Eq. 1, we can easily find the expression for contrast change over the distances (m) that is found in most target acquisition and sensor performance models:

$$c(s) = \frac{C(0)}{1 + \left(\frac{L_s}{L_b(0)}\right)\left(\frac{1}{T(s)} - 1\right)} \quad (5)$$

The ratio of limiting path radiance Ls to zero-range background radiance $L_b(0)$ is the (usually input) "sky-to-ground ratio" Sg:

$$S_g = L_s / L_b(0) \quad (6)$$

The origins of the Sg inputs to models and simulations can be observations, models or simply "ad-hoc" values for scenarios. Observations, which are valid for near horizontal lines of sight, use the ratio of the sky radiance L_s just above the horizon to the background radiance $L_b(0)$ observed from the target location. These properly account for sun position and "sun at back" versus "sun in eyes" differences in contrast. However, they are usually meaningless at night except under moonlit conditions. Then the ratios of radiance from scattering by the atmosphere (L_s) to reflection from terrain (L_b) scale about the same regardless of whether the sun or the moon is the illumination source. Models can also be effective for daytime and moonlit conditions to treat non-horizontal lines of sight. However, it is still very common to see the use of "typical scenario" Sg as input constants. Daylight values for Sg are 3 to 5 for objects viewed against terrain, one for an object viewed against the horizon sky, and 6 to 9 when viewing near the sun and into the glare of sunlight through haze.

This situation is, of course, more complicated when the primary illumination source is a flare at night, and when obscurants such as smoke and dust produce the scattering. Then simple estimates no longer apply. However, long, detailed modeling runs are often impractical. Some combination of simplified model and interpolation in pre-computed tables is required. In the following sections we outline some of the results of a project to develop such a capability as part of an on-going process in the TRADOC Target Acquisition Simulation (ACQSIM) program and between TRAC-WSMR and the Army Research Laboratory (ARL).

AN EARLIER MODEL - COIL

The effects on contrast of an object against a background not only varies with the flare illumination dependence on range, but also on the scattering and attenuation effects of the atmosphere from flare to object (and background) and from object (and background) to the sensor. In 1975 ARPA funded a model through General Research Corporation called the Combat Illumination (COIL) model (Stathacopoulos, 1975). The COIL documentation shows that it was meant to treat the basic problem of flare geometry, terrain reflectance, and simple attenuation and scattering from a uniform atmosphere. The methods were rather crude in that radiance reaching an object was estimated by sampling along only 20 rays, including that from the flare, and most reflectance and scattering (even from terrain) was considered as isotropic into a sphere or hemisphere. The COIL computer code is apparently no longer available, however, and thus the present project was begun.

BLACK SKY BACKGROUNDS

What value of Sg should be used for night-time contrast under natural illumination and under flare illumination? Determining this value is a major goal of the present effort.

One problem is that for a black background sky or distant non-illuminated terrain, then $L_b(0)$ is zero. Thus, the required input Sg ratio L_s/L_b is infinite [as is the zero range contrast C(0)].

One solution is to allow the user to continue to choose any finite value of C(0), and then to specify an accurate illuminated object radiance LO(0). Then the physically-consistent value for Sg should be:

$$S_g = L_s \cdot \left[1 + C(0)\right] / L_o(0) \quad (7)$$

Or we can assume that the background radiance at the sensor is never less than the limiting sensor noise value. Thus if $L_b(0)$ is arbitrarily chosen as this lower limit (say a micro-watt/m^2/sr), then Eqs. 1 and 5 can consistently be used for contrast C(0) and Sg. Before considering the effects of obscurants, however, we must first treat modeling of flare-illuminated object and background radiances.

DIRECT FLARE RADIANCE

As shown in Fig. 1, we treat a single flare as a point source of radiant power (also known as the radiant flux) P_s' (watts W) at a height h_s (m) above the terrain. Define any surface directly illuminated by the flare at a height h_f' (m) above the terrain and at a ground surface range R_f' (m) from the ground point directly below the flare. (The use of "primes" on the various quantities will be made clear shortly, when we reintroduce them as scaled parameters,) The surface orientation is defined by a surface normal vector that makes an angle θ with the vector from the surface to the flare. The surface can be any terrain element or an object facet. We assume for this paper that the flare emits power equally in all directions (4π steradians sr). Thus, the radiant intensity I_s' (W/sr) of the flare is:

$$I'_s = P'_s / (4\pi) \qquad (8)$$

We will use ANSI (1986) radiometric units (W, W/sr, W/m^2, and W/m^2/sr) in favor of photometric units in this paper. Corresponding photometric units (lumens, candelas, lux, and cd/m^2) require band-integration over the photopic or scotopic spectral responses of the eye. A nice discussion of the ANSI definitions of radiometric and photometric units is given in the appendix of Ashdown (1994). The surface irradiance E_f' (W/m^2) depends on the surface's distance to the flare and on the cosine of the angle between the surface normal and the ray from the surface to the flare. In terms of the surface-normal direction cosines μ_f, i.e. $(\alpha_f, \beta_f, \gamma_f)$ and the direction cosines of the ray from the surface field point to the flare μ_s, i.e. $(\alpha_s, \beta_s, \gamma_s)$:

$$E'_f = \left(\frac{P'_s}{1000}\right) \cdot \frac{1000 \cdot (\mu_s \circ \mu_f)}{4\pi \left((h_s - h'_f)^2 + R'^2_f\right)} \qquad (9)$$

where components are defined in terms of source and field point coordinates (x,', y,', z,') and (x_f', y_f', z_f'):

$$\mu_s \circ \mu_f = \alpha_s \cdot \alpha_f + \beta_s \cdot \beta_f + \gamma_s \cdot \gamma_f \qquad (10)$$

$$\alpha_s = \frac{x'_s - x'_f}{\sqrt{(h_s - h;\ )^2 + R'^2_f}} = \frac{x_s - x_f}{\sqrt{(1 - h_f)^2 + R_f^2}} \qquad (11)$$

$$\beta_s = \frac{y'_s - y'_f}{(h_s - h'_f)^2 + R'^2_f} = \frac{y_s - y_f}{\sqrt{(1 - h_f)^2 + R_f^2}} \qquad (12)$$

$$\gamma_s = \frac{z'_s - z'_f}{(h_s - h'_f)^2 + R'^2_f} \qquad (13)$$

In the above, x, y, z, h_f and R_f are "scaled distances" (each dimensionless) in terms of the source height. Distances are thus now expressed simply as the number of "flare heights" or "h_s units" as:

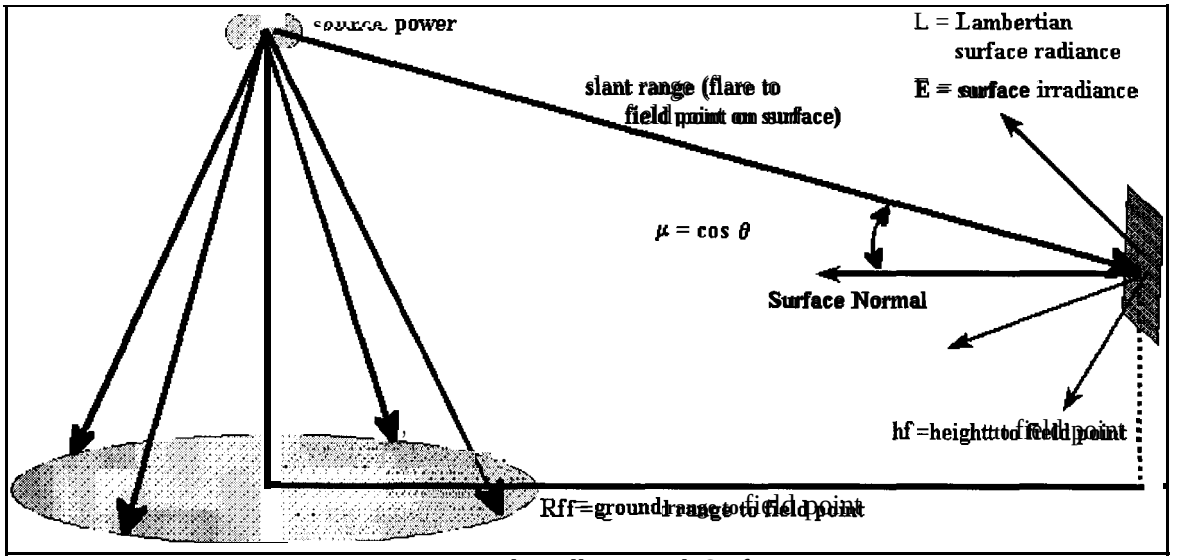

Figure 1. Flare-Illuminated Surfaces

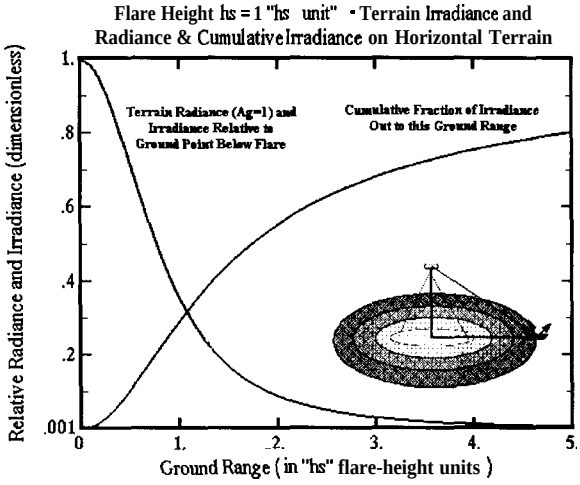

Figure 2. Relative Terrain Surface Irradiance

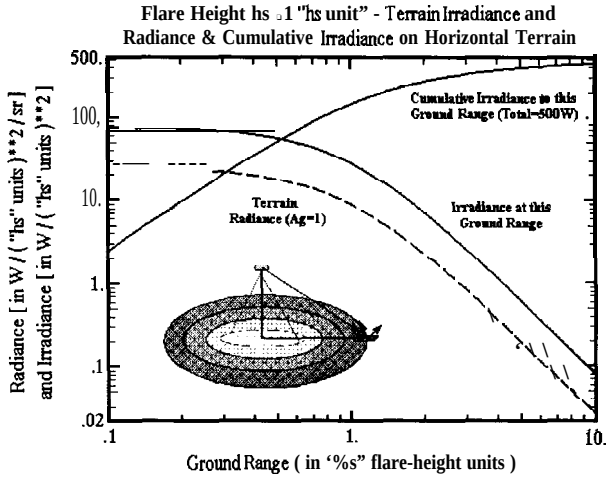

Figure 3. Diffuse Terrain Irradiance and Radiance

$$x' = x \cdot h_s\,,\quad y' = y \cdot h_s\,,\quad z' = z \cdot h_s \qquad (14)$$

$$h_f' = h_f \cdot h_s\,,\quad R_f' = R_f \cdot h_s \qquad (15)$$

while the "scaled irradiance" E_f (dimensionless) in terms of a 1000 W source and "h, units" is:

$$E_f' = \frac{P_s'}{1000 \cdot h_s^2} E_f \qquad (16)$$

and where the study now concentrates on computing:

$$E_f = \frac{1000 \cdot (\mu_s \circ \mu_f)}{4\pi\,(1 + R_f^2)} \qquad (17)$$

The advantage of using these scaling methods is that we then need only compute the problem for a single flare power (i.e. 1000 W) and a "unit flare height" (i.e., $h_s = 1$). Now if the irradiated surface is Lambertian with reflectance A_f, (dimensionless from O to 1), then it diffusely reflects the illumination, producing its own scaled radiance (sr^{-1}) in all directions:

$$L_f = A_f \cdot E_f \,/\, \pi \qquad (18)$$

and correspondingly, the actual radiance ($W/m^2/sr$):

$$L_f' = A_f \cdot E_f' \,/\, \pi \qquad (19)$$

Figure 2 plots the computed relative values of E_f (and, in fact, the direct radiance contribution to L_f) for the horizontal terrain surface and a terrain reflectance

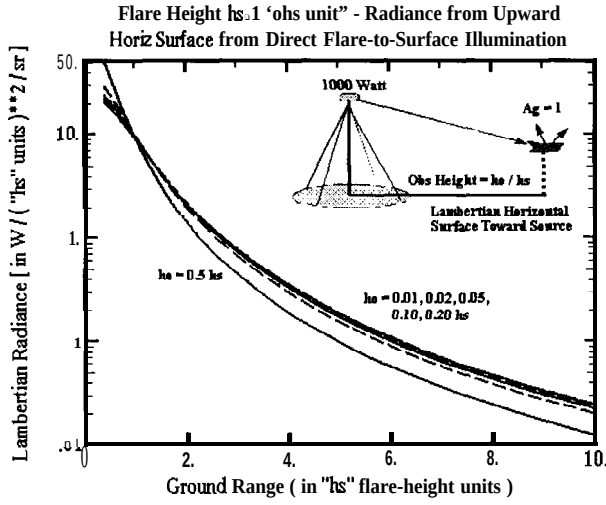

Figure 4. Horizontal Surface radiance - Direct

(albedo) of one. The horizontal axis is the scaled ground distance R_f from the flare. It can be seen that the surface irradiances and reflected radiances fall to 35%,9% and 3% of the maximum at radii of just one, two and three flare heights respectively. However, even at a ground distance of five flare heights, where the relative irradiance and radiance are reduced to 0.1 % of the maximum, only 80% of all the downward flare radiant power has illuminated the surface. The remaining 20% of the total downward radiated power is spread over the rest of the very large surrounding area.

Figure 3 shows the actual (scaled) irradiance E_b and radiance Lb for the terrain (using subscript "b" for "background") in $W/(h_s^2)/sr$ for the 1000 W reference source and a ground albedo of one. Figure 4 shows the reflected radiance due to direct radiance from the flare for any other upward-facing horizontal object surface at scaled height h_o with scaled ground range in h_s units.

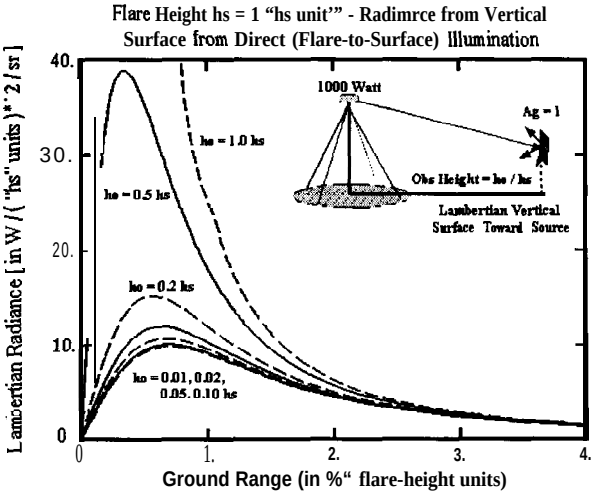

Figure 5. Vertical Surface Radiance - from Direct

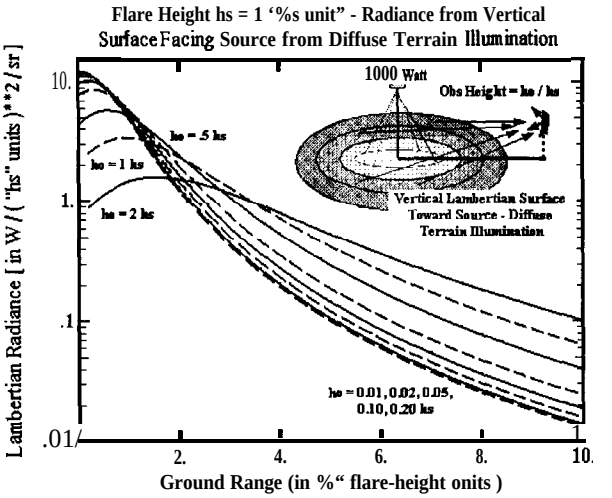

Figure 6. Vertical Surface Radiance -Diffuse

Figure 5 shows the reflected radiance due to direct flare illumination for any vertical surface that is rotated around the z-axis to face the flare. Note that as a horizontal surface (Fig. 4) is raised to about half the flare height there is little change in reflected radiance. However, vertical surface radiance (Fig. 5) shows strong dependence on height above the terrain (especially out to two or three flare-height radii) due to the dot product of the illumination ray with the surface normal.

DIFFUSE RADIANCE

Direct illumination from the flare (if any) is the dominant source of reflected radiance from surfaces such as targets above the terrain. However, the diffuse irradiance from the terrain itself can also be an important factor. To compute this contribution one must integrate the incident radiance L_b from all terrain surface elements in the relevant directions and at all ranges:

$$E_o = \int \frac{(\mu \circ \mu_o)\gamma_b}{(x - x_o)^2 + (y - y_o)^2 + h_o^2} L_b(x,y)\, dx\, dy \qquad (20)$$

where (x_o, y_o, h_o) are the coordinates of the diffusely illuminated "object surface", μ_o is the object surface normal dotted with the direction cosines of the ray from the object to the terrain element "dx dy" at position (x, y, z), and γ_b is the z-component direction cosine of the ray with respect to the normal to the terrain element. The corresponding radiance from the object surface is:

$$L_o = A_o E_o / \pi \qquad (21)$$

Because of the complexity of the above integral, data have been numerically computed for object

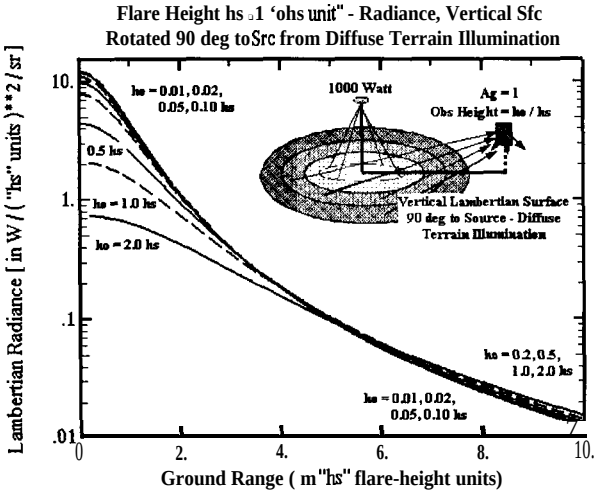

Figure 7. Vertical Surface Radiance - Diffuse

surfaces at various orientations. A few are shown in the following figures. Figure 6 shows the radiance contribution originating from diffuse terrain radiance and reflected from any vertical object surface rotated about the vertical axis to face the flare. Figure 7 is similar, but for the vertical object surface rotated at right angles to the flare (i.e., edge-on). Figure 8 is for the vertical object surface rotated to face away from the flare. Figure 9 shows the contribution of terrain diffuse radiance on the reflected radiance from any downward facing horizontal surface.

Although there are considerable differences in the diffuse terrain radiance contributions seen in these figures, these differences are mostly at the large object heights (0.5, 1.0 and 2.0 flare-heights) and at small distances from the flare. It is interesting that at large radial distances, the object surface radiances are fairly comparable, regardless of object orientation, and the

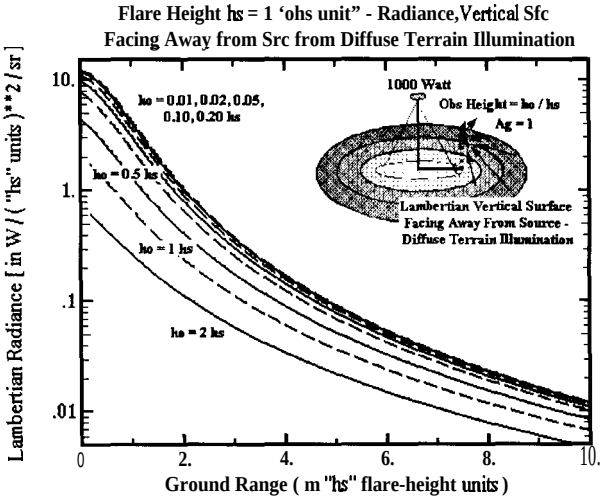

Figure 8. Vertical Surface Radiance - Diffuse

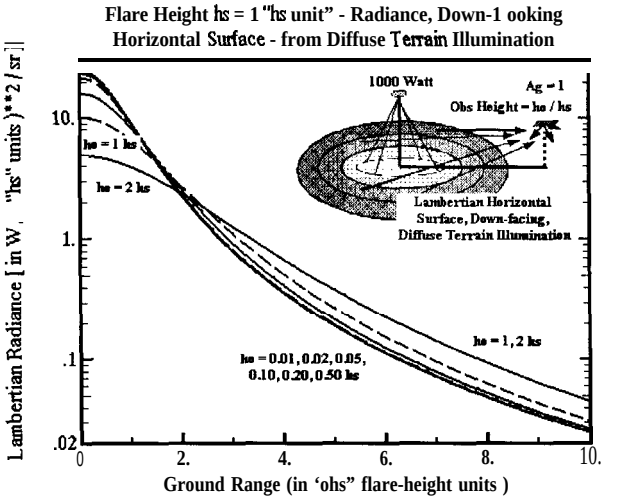

Figure 9. Horizontal Surface Radiance - Diffuse

direct radiance contributions are not appreciably larger than the diffuse contributions. At small radial distances of a few flare heights the direct illumination dominates, of course, especially as the object height is raised above the terrain. And, since the computations are for terrain and object surface albedos of one, we must also note that the direct-radiance contribution will scale as A_o (object albedo), while the diffuse contribution will scale as $A_o * A_b$ (object albedo times terrain albedo).

In the current modeling study we actually compute and store the diffuse radiance for several more surface orientations. These tables are used to interpolate to any general orientation. The contributions of direct radiance are easily computed on the fly using the direct radiance equations of the earlier section.

CLOUD TRANSMISSION AND RADIANCE

Having defined all the quantities required for flare illumination of backgrounds (Lb) and objects (LO) in an unobscured environment, we can compute the contrast C at any point. However, we now turn to modeling the transmittance T and the limiting path radiance L_s numerator in the Sg term.

Models for smoke and dust transmittance (Ayres, 1993) are available from the Electro-Optical Systems Atmospheric Effects Library (EOSAEL, 1987). The Battlefield Emission and Multiple scattering (BEAMS) Model (Hoock, et. al. 1993, 1994, 1995; O'Brien, 1993) computes the radiance through smoke and dust clouds. In the present project we used BEAMS to compute L_s for the scattering from uniform cloud blocks 48 m long, 32 m wide and 16 m high of fog oil, phosphorus and dust. Optical depths of the clouds were varied from 0.25 to 64 across the cloud width. A 1000

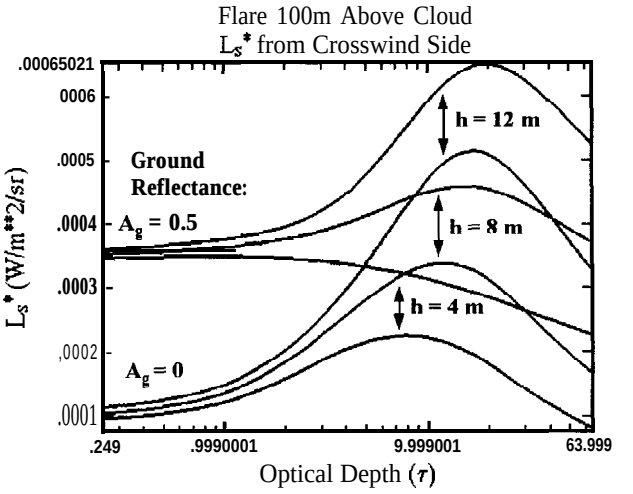

Figure 10. Cloud Ls Radiance from Sides

W flare was placed at four different locations in separate runs: directly above the cloud center at 116 m, 24m and 8 m above ground level; and for an off-axis location 62 m above the surface and 93.5 m in ground distance from the cloud center. The entire set of 60 runs were repeated for terrain albedos of zero (no terrain) and 0.5.

The analyzed radiances are being stored as tables and parametric curves. Figure 10 is an example of L_s exiting the side of a fog oil cloud with the flare 116 m above the terrain (100m above the top center of the cloud). Figures 11 and 12 show L_s values for radiance "- from the bottom and from the top of the cloud respectively. Note that radiance from the side of the cloud varies with height of the exit point for optically thick smoke. This quantifies the darkening near the bottom due to obscuration as radiant power is lost from the side of the cloud. The radiance exiting the bottom of the cloud shows only a small dependence on terrain albedo. The difference is due to diffusely reflected

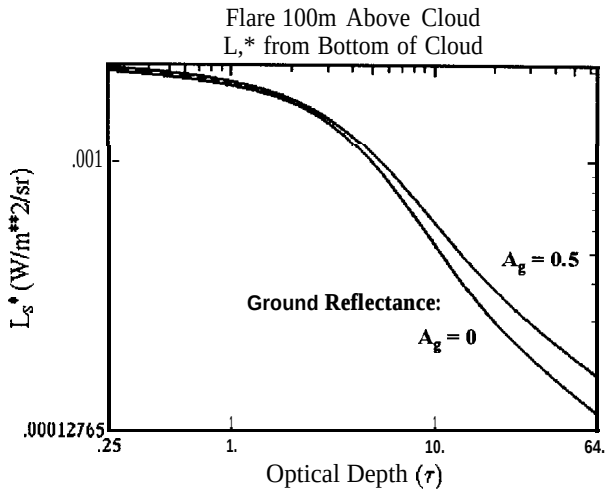

Figure 11. Cloud Ls Radiance from Bottom

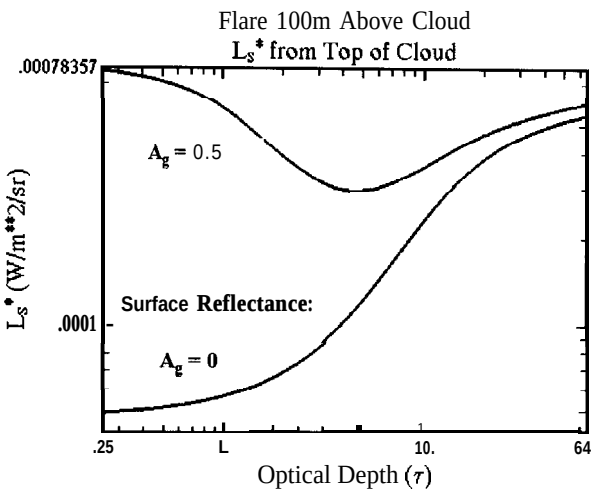

Figure 12. Cloud Ls Radiance from Top

terrain radiance back-scattered from the cloud. The large variation with albedo for radiance exiting the top of the cloud is due to the reflected terrain radiance that is only partly obscured at small optical depths.

Examples of cloud appearance are shown in Figs. 13 through 17. Figure 13 is the uniform rectangular fog oil cloud used to generate the tables and parametric curves for Ls in the study. (The ringed appearance is due to gray-level quantization in the figures in this paper.) Figure 14 shows a non-uniform fog oil cloud with optical depth of one across the 32 m width (top) and Opticaf Depth (OD) of four (bottom). The flare is at 116 m altitude directly above the cloud.

Figure 15 shows the flare at 30 deg elevation and 108 m range from the cloud. Cloud width OD's are one (bottom) and four (top). Figures 16 and 17 show the case of the flare just 8 m above the cloud surface for OD'S of one and four respectively.

Current efforts are to better account in the parameterized data for the cloud shadow regions which alter the diffuse radiance as well as direct radiance.

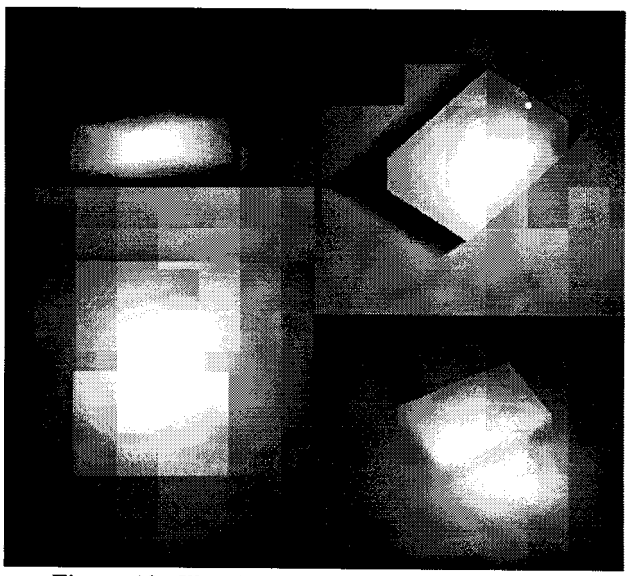

Figure 13. Illuminated Uniform Fog Oil Cloud

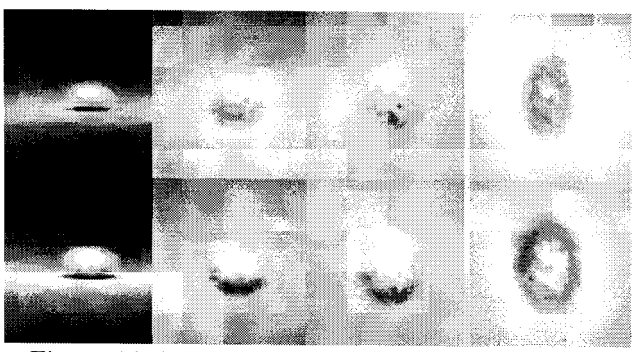

Figure 14. Flare at (0 m, 0 m, 116 m) on Fog Oil. Top Optical Depth = 1, Bottom OD = 4.

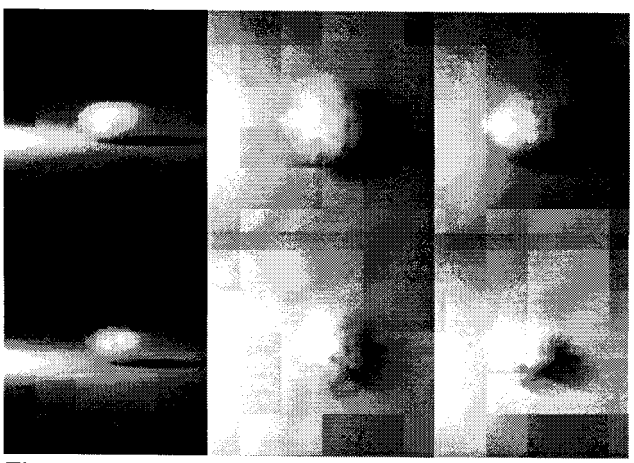

Figure 15. Flare at (0 m, 93.5m, 62m) on Fog Oil. Top Optical Depth = 4, Bottom OD = 1.

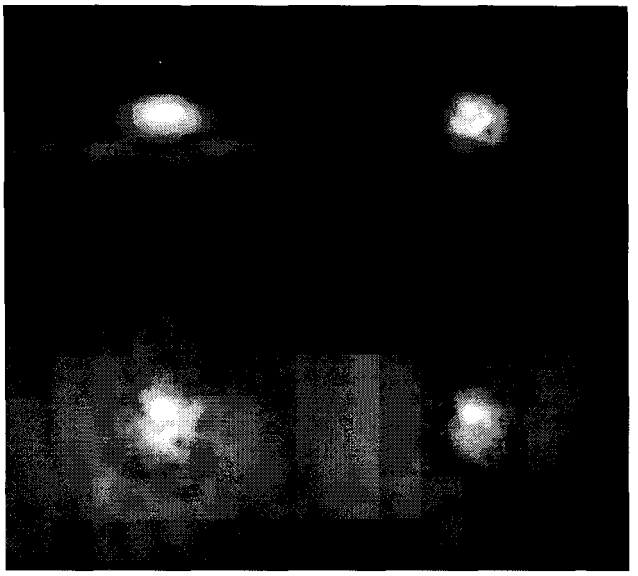

Figure 16. Illumination for Flare 8 m Above Fog Oil Cloud of Optical depth= 1

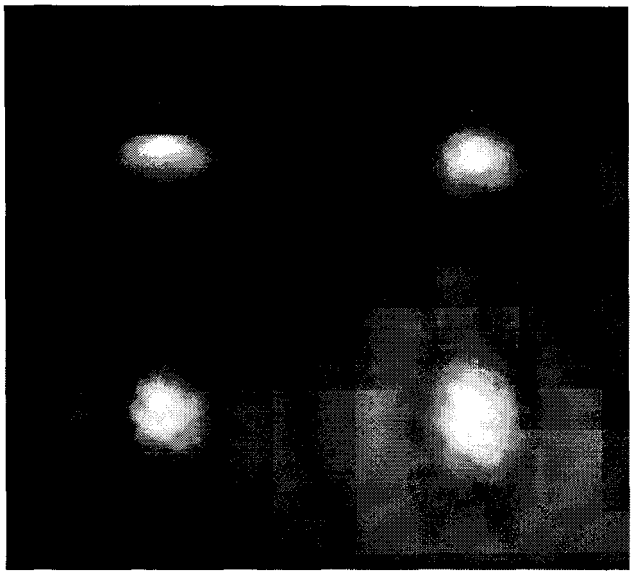

Figure 17. Illumination for Flare 8 m Above Fog Oil Cloud of Optical depth= 4

A CONTRAST EXAMPLE

Figure 18 shows an example of the changes in contrast under a flare with and without a smoke cloud. The scenario is that of a vertical-surface (object) moving toward an observer whose line of sight is a constant 1 deg elevation above the terrain. The object begins at a ground range 9 flare heights beyond the flare (point"18" on the horizontal axis), moves toward the observer and passes beneath the flare (point "9" on the axis) and finally ceases movement at a ground range of 9 "flare heights" on the observer side of the flare (point "O").

Contrast varies from minus one (a black object against a bright background) through zero (no contrast between the object and background) and to positive infinity (bright object against a black background). In order to plot this range on a log scale, we have added a constant value of one to all contrasts displayed on the vertical axis of the plot. Thus, any value of (1 +C) less than one is a negative (dark object on light background) contrast. Any value of (1+C) greater than one is a positive (light object on a dark background) contrast

$$\log_{10}\left[1+C(s)\right] = \log_{10}\left[L_o(s)\right] - k\%_o\left[L_b(s)\right] \quad (22)$$

The example is for a 1000 W flare at 116 m above the surface. The object is 2.3 m above the terrain. Both the object and terrain have albedos of 0.5. The solid line shows that even though the reflectance are equal, the different distances of the object and the background from the observer generates a significant contrast. It is approximately 12 at the most distant point. The contrast falls slowly to about half the initial value at 2 flare-heights beyond the flare. It then falls to 0.35 contrast (or 1.35 on the vertical axis) as it passes below the flare (9 on the horizontal axis). At this point the object is illuminated only by diffuse terrain radiance from the observer side of the flare. The contrast then goes negative (less than one on the vertical axis) at about 0.15 flare heights on the observer side of the flare. As the object proceeds toward the zero point on the horizontal axis, the contrast falls to about -0.89 at 2 flare heights on the observer side (7 on the horizontal axis). Actually at this point the object attains its "best" negative contrast. As it continues to move toward the observer, the contrast again rises to a final value of -0.66 (at O on the horizontal axis).

Now consider the dashed line. This plot of "contrast+ 1" shows the immediate effect of smoke obscuration that extends from about 7 source heights beyond the cloud (16 on the horizontal axis) to about 1.5 source heights on the observer side (7.5 on the horizontal axis). The smoke cloud is 16 m high and has an optical depth of one. It intercepts the line of sight over this range. Interestingly, while the contrast falls as the object approaches the flare in the "clear air" case, it actually rises slightly in the presence of the smoke. In part this is because the cloud itself is a source of radiance that illuminates the object more than the distant background point. The fluctuating behavior as the object approaches the cloud is due in part to the shadow of the cloud, the obscuration of the diffuse terrain on the far side of the

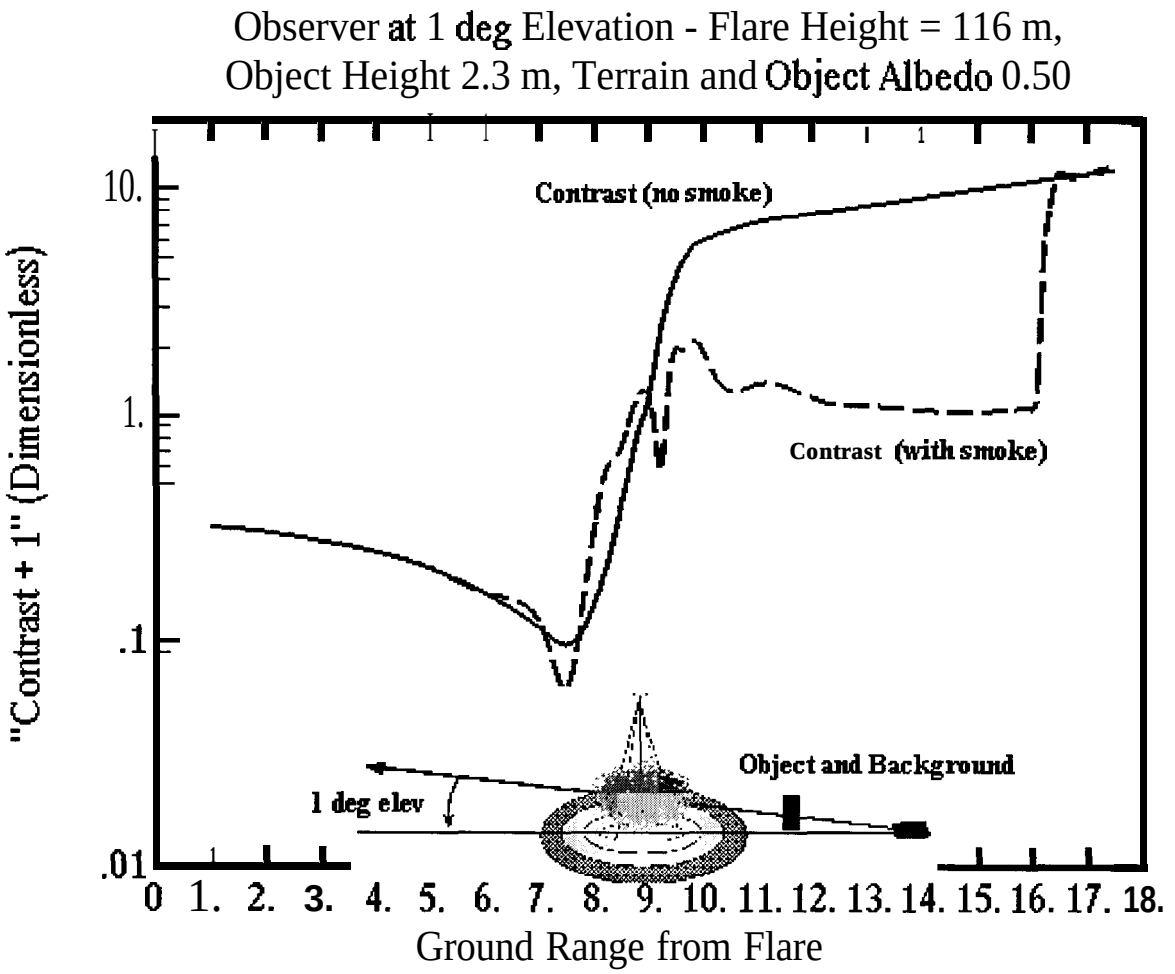

Figure 18. Example of Object Contrast Under Flare and Smoke

cloud, and the changing path length of obscurant in front of the object as it passes through and out of the cloud. The background "lags behind" the object in its passage through the cloud. Thus, for a short distance the background is obscured while the object is not obscured. By the point where both the object and background are not influenced significantly by the cloud (at about 2 source heights on the observer side of the cloud) the contrast again attains the clear air value.

Of course, the behavior under any other set of circumstances can be different. The effects are highly dependent on geometry. We should also note that the treatment of the shadow area around the flare is still being finalized. Thus, details of variations near the smoke should be considered with caution.

CONCLUSIONS

Radiometrically correct simulation of night-time conditions on visual systems is made difficult when the primary illumination is artificial. We have outlined here a project to develop a practical, parametrized model based on research model outputs. The problem of providing input contrast and sky-to-ground ratios to the standard contrast algorithms used in constructive simulations is made much more complicated by the presence of aerosols. And rendering of scenes in real-time virtual simulations with sufficient correlation to the effects used in constructive simulation is complicated primarily by the need to properly account for diffuse radiance and cloud shadowing. In fact the proper parameterization of the shadowing effect is the final aspect in the current project that was still being addressed as this paper was submitted.

ACKNOWLEDGMENTS

We wish to acknowledge the support of TRAC-WSMR in this project and the efforts of the TRAC-lead ACQSIM group for coordinating improvements in target acquisition simulation.

REFERENCES

ANSI/IES (1986). American National Standard Nomenclature and definitions for Illumination Engineering, ANSI/IES RP- 16-1986, Illumination Engineering Society of North America, New York.

Ashdown, Ian (1994). Radiosity, A Programmer's Perspective. John Wiley and Sons, New York

Ayres, Scarlett and DeSutter, S. (1993). EOSAEL 92: Vol 14. Combined Obscuration Model for Battlefield-Induced Contaminants (COMBIC), U.S. -Army Research Laboratory Report, Adelphi, MD.

Hoock, D., Giever, J. & OBrien, S (1993). Battlefield Emission and Multiple Scattering (BEAMS), a 3-D Inhomogeneous Radiance Transfer Model, Proceedings of the SPIE, 1967, 268-277. Bellingham, WA: SPIE -- The International Society for Optical Engineering.

Hoock, D. & Giever, J. (1994). Modeling Effects of Terrain and Illumination on Visibility and the Visualization of Haze and Aerosols, Proceedings of the SPIE, 2223, 450-461. Bellingham, WA: SPIE -- The International Society for Optical Engineering.

Hoock, Donald, O'Brien, S., Giever, J. and McGee, S. (1995). High Fidelity Modeling of Obscurants for Virtual and Constructive Simulations, Proceedings of the 1995 ITEA Workshop "Modeling and Simulation: Today and Tomorrow", White Sands Missile Range, NM.

O'Brien, S. (1993). Comparison of the BEAMS 2.2 Radiative Transfer Algorithm with Other Radiative Transfer Methods, Proceedings of the 1993 Battlefield Atmospherics Conference, U.S. Army Research Laboratory, Battlefield Environment Directorate, White Sands Missile Range, NM, 421-435.

Shirkey, Richard, Duncan, L. and Niles, F. (1987). Executive Summary, EOSAEL 87, Vol 1, ASL-TR-0221-1, U.S. Army Research Lab, Adelphi, MD.

Strathacopoulos, A., Gilmore H., Czipott A., Gordon, C. and Rohringer, G. (1975). Combat Illumination Model (COIL), CRC Contractor Report CR-2-548, (DTIC ADBOO661O), General Research Corp., Santa Barbara, CA.